11-8-2006

Measurement of the *CP*-violation parameter of B^0 mixing and decay with $p\bar{p} \rightarrow \mu\mu X$ data

V. M. Abazov
Joint Institute for Nuclear Research, Dubna, Russia

Kenneth A. Bloom
University of Nebraska-Lincoln, kenbloom@unl.edu

Gregory R. Snow
University of Nebraska-Lincoln, gsnow1@unl.edu

D0 Collaboration

Measurement of the *CP*-violation parameter of B^0 mixing and decay with $p\bar{p} \rightarrow \mu\mu X$ data

V. M. Abazov,[35] B. Abbott,[75] M. Abolins,[65] B. S. Acharya,[28] M. Adams,[51] T. Adams,[49] M. Agelou,[17] E. Aguilo,[5] S. H. Ahn,[30] M. Ahsan,[59] G. D. Alexeev,[35] G. Alkhazov,[39] A. Alton,[64] G. Alverson,[63] G. A. Alves,[2] M. Anastasoaie,[34] T. Andeen,[53] S. Anderson,[45] B. Andrieu,[16] M. S. Anzelc,[53] Y. Arnoud,[13] M. Arov,[52] A. Askew,[49] B. Åsman,[40] A. C. S. Assis Jesus,[3] O. Atramentov,[49] C. Autermann,[20] C. Avila,[7] C. Ay,[23] F. Badaud,[12] A. Baden,[61] L. Bagby,[52] B. Baldin,[50] D. V. Bandurin,[59] P. Banerjee,[28] S. Banerjee,[28] E. Barberis,[63] P. Bargassa,[80] P. Baringer,[58] C. Barnes,[43] J. Barreto,[2] J. F. Bartlett,[50] U. Bassler,[16] D. Bauer,[43] S. Beale,[5] A. Bean,[58] M. Begalli,[3] M. Begel,[71] C. Belanger-Champagne,[5] L. Bellantoni,[50] A. Bellavance,[67] J. A. Benitez,[65] S. B. Beri,[26] G. Bernardi,[16] R. Bernhard,[41] L. Berntzon,[14] I. Bertram,[42] M. Besançon,[17] R. Beuselinck,[43] V. A. Bezzubov,[38] P. C. Bhat,[50] V. Bhatnagar,[26] M. Binder,[24] C. Biscarat,[42] K. M. Black,[62] I. Blackler,[43] G. Blazey,[52] F. Blekman,[43] S. Blessing,[49] D. Bloch,[18] K. Bloom,[67] U. Blumenschein,[22] A. Boehnlein,[50] O. Boeriu,[55] T. A. Bolton,[59] G. Borissov,[42] K. Bos,[33] T. Bose,[77] A. Brandt,[78] R. Brock,[65] G. Brooijmans,[70] A. Bross,[50] D. Brown,[78] N. J. Buchanan,[49] D. Buchholz,[53] M. Buehler,[81] V. Buescher,[22] S. Burdin,[50] S. Burke,[45] T. H. Burnett,[82] E. Busato,[16] C. P. Buszello,[43] J. M. Butler,[62] P. Calfayan,[24] S. Calvet,[14] J. Cammin,[71] S. Caron,[33] W. Carvalho,[3] B. C. K. Casey,[77] N. M. Cason,[55] H. Castilla-Valdez,[32] S. Chakrabarti,[28] D. Chakraborty,[52] K. M. Chan,[71] A. Chandra,[48] F. Charles,[18] E. Cheu,[45] F. Chevallier,[13] D. K. Cho,[62] S. Choi,[31] B. Choudhary,[27] L. Christofek,[77] D. Claes,[67] B. Clément,[18] C. Clément,[40] Y. Coadou,[5] M. Cooke,[80] W. E. Cooper,[50] D. Coppage,[58] M. Corcoran,[80] M.-C. Cousinou,[14] B. Cox,[44] S. Crépé-Renaudin,[13] D. Cutts,[77] M. Ćwiok,[29] H. da Motta,[2] A. Das,[62] M. Das,[60] B. Davies,[42] G. Davies,[43] G. A. Davis,[53] K. De,[78] P. de Jong,[33] S. J. de Jong,[34] E. De La Cruz-Burelo,[64] C. De Oliveira Martins,[3] J. D. Degenhardt,[64] F. Déliot,[17] M. Demarteau,[50] R. Demina,[71] P. Demine,[17] D. Denisov,[50] S. P. Denisov,[38] S. Desai,[72] H. T. Diehl,[50] M. Diesburg,[50] M. Doidge,[42] A. Dominguez,[67] H. Dong,[72] L. V. Dudko,[37] L. Duflot,[15] S. R. Dugad,[28] D. Duggan,[49] A. Duperrin,[14] J. Dyer,[65] A. Dyshkant,[52] M. Eads,[67] D. Edmunds,[65] T. Edwards,[44] J. Ellison,[48] J. Elmsheuser,[24] V. D. Elvira,[50] S. Eno,[61] P. Ermolov,[37] H. Evans,[54] A. Evdokimov,[36] V. N. Evdokimov,[38] S. N. Fatakia,[62] L. Feligioni,[62] A. V. Ferapontov,[59] T. Ferbel,[71] F. Fiedler,[24] F. Filthaut,[34] W. Fisher,[50] H. E. Fisk,[50] I. Fleck,[22] M. Ford,[44] M. Fortner,[52] H. Fox,[22] S. Fu,[50] S. Fuess,[50] T. Gadfort,[82] C. F. Galea,[34] E. Gallas,[50] E. Galyaev,[55] C. Garcia,[71] A. Garcia-Bellido,[82] J. Gardner,[58] V. Gavrilov,[36] A. Gay,[18] P. Gay,[12] D. Gelé,[18] R. Gelhaus,[48] C. E. Gerber,[51] Y. Gershtein,[49] D. Gillberg,[5] G. Ginther,[71] N. Gollub,[40] B. Gómez,[7] A. Goussiou,[55] P. D. Grannis,[72] H. Greenlee,[50] Z. D. Greenwood,[60] E. M. Gregores,[4] G. Grenier,[19] Ph. Gris,[12] J.-F. Grivaz,[15] S. Grünendahl,[50] M. W. Grünewald,[29] F. Guo,[72] J. Guo,[72] G. Gutierrez,[50] P. Gutierrez,[75] A. Haas,[70] N. J. Hadley,[61] P. Haefner,[24] S. Hagopian,[49] J. Haley,[68] I. Hall,[75] R. E. Hall,[47] L. Han,[6] K. Hanagaki,[50] P. Hansson,[40] K. Harder,[59] A. Harel,[71] R. Harrington,[63] J. M. Hauptman,[57] R. Hauser,[65] J. Hays,[53] T. Hebbeker,[20] D. Hedin,[52] J. G. Hegeman,[33] J. M. Heinmiller,[51] A. P. Heinson,[48] U. Heintz,[62] C. Hensel,[58] K. Herner,[72] G. Hesketh,[63] M. D. Hildreth,[55] R. Hirosky,[81] J. D. Hobbs,[72] B. Hoeneisen,[11] H. Hoeth,[25] M. Hohlfeld,[15] S. J. Hong,[30] R. Hooper,[77] P. Houben,[33] Y. Hu,[72] Z. Hubacek,[9] V. Hynek,[8] I. Iashvili,[69] R. Illingworth,[50] A. S. Ito,[50] S. Jabeen,[62] M. Jaffré,[15] S. Jain,[75] K. Jakobs,[22] C. Jarvis,[61] A. Jenkins,[43] R. Jesik,[43] K. Johns,[45] C. Johnson,[70] M. Johnson,[50] A. Jonckheere,[50] P. Jonsson,[43] A. Juste,[50] D. Käfer,[20] S. Kahn,[73] E. Kajfasz,[14] A. M. Kalinin,[35] J. M. Kalk,[60] J. R. Kalk,[65] S. Kappler,[20] D. Karmanov,[37] J. Kasper,[62] P. Kasper,[50] I. Katsanos,[70] D. Kau,[49] R. Kaur,[26] R. Kehoe,[79] S. Kermiche,[14] N. Khalatyan,[62] A. Khanov,[76] A. Kharchilava,[69] Y. M. Kharzheev,[35] D. Khatidze,[70] H. Kim,[78] T. J. Kim,[30] M. H. Kirby,[34] B. Klima,[50] J. M. Kohli,[26] J.-P. Konrath,[22] M. Kopal,[75] V. M. Korablev,[38] J. Kotcher,[73] B. Kothari,[70] A. Koubarovsky,[37] A. V. Kozelov,[38] D. Krop,[54] A. Kryemadhi,[81] T. Kuhl,[23] A. Kumar,[69] S. Kunori,[61] A. Kupco,[10] T. Kurča,[19,*] J. Kvita,[8] S. Lammers,[70] G. Landsberg,[77] J. Lazoflores,[49] A.-C. Le Bihan,[18] P. Lebrun,[19] W. M. Lee,[52] A. Leflat,[37] F. Lehner,[41] V. Lesne,[12] J. Leveque,[45] P. Lewis,[43] J. Li,[78] Q. Z. Li,[50] J. G. R. Lima,[52] D. Lincoln,[50] J. Linnemann,[65] V. V. Lipaev,[38] R. Lipton,[50] Z. Liu,[50] L. Lobo,[43] A. Lobodenko,[39] M. Lokajicek,[10] A. Lounis,[18] P. Love,[42] H. J. Lubatti,[82] M. Lynker,[55] A. L. Lyon,[50] A. K. A. Maciel,[2] R. J. Madaras,[46] P. Mättig,[25] C. Magass,[20] A. Magerkurth,[64] A.-M. Magnan,[13] N. Makovec,[15] P. K. Mal,[55] H. B. Malbouisson,[3] S. Malik,[67] V. L. Malyshev,[35] H. S. Mao,[50] Y. Maravin,[59] M. Martens,[50] R. McCarthy,[72] D. Meder,[23] A. Melnitchouk,[66] A. Mendes,[14] L. Mendoza,[7] M. Merkin,[37] K. W. Merritt,[50] A. Meyer,[20] J. Meyer,[21] M. Michaut,[17] H. Miettinen,[80] T. Millet,[19] J. Mitrevski,[70] J. Molina,[3] N. K. Mondal,[28] J. Monk,[44] R. W. Moore,[5] T. Moulik,[58] G. S. Muanza,[15] M. Mulders,[50] M. Mulhearn,[70] O. Mundal,[22] L. Mundim,[3] Y. D. Mutaf,[72] E. Nagy,[14] M. Naimuddin,[27] M. Narain,[62] N. A. Naumann,[34] H. A. Neal,[64] J. P. Negret,[7] P. Neustroev,[39] C. Noeding,[22] A. Nomerotski,[50] S. F. Novaes,[4] T. Nunnemann,[24] V. O'Dell,[50] D. C. O'Neil,[50] G. Obrant,[39] V. Oguri,[3] N. Oliveira,[3] D. Onoprienko,[59] N. Oshima,[50] R. Otec,[9] G. J. Otero y Garzón,[51] M. Owen,[44] P. Padley,[80] N. Parashar,[56] S.-J. Park,[71] S. K. Park,[30] J. Parsons,[70] R. Partridge,[77] N. Parua,[72] A. Patwa,[73] G. Pawloski,[80] P. M. Perea,[48] E. Perez,[17] K. Peters,[44]

P. Pétroff,[15] M. Petteni,[43] R. Piegaia,[1] J. Piper,[65] M.-A. Pleier,[21] P. L. M. Podesta-Lerma,[32] V. M. Podstavkov,[50] Y. Pogorelov,[55] M.-E. Pol,[2] A. Pompoš,[75] B. G. Pope,[65] A. V. Popov,[38] C. Potter,[5] W. L. Prado da Silva,[3] H. B. Prosper,[49] S. Protopopescu,[73] J. Qian,[64] A. Quadt,[21] B. Quinn,[66] M. S. Rangel,[2] K. J. Rani,[28] K. Ranjan,[27] P. N. Ratoff,[42] P. Renkel,[79] S. Reucroft,[63] M. Rijssenbeek,[72] I. Ripp-Baudot,[18] F. Rizatdinova,[76] S. Robinson,[43] R. F. Rodrigues,[3] C. Royon,[17] P. Rubinov,[50] R. Ruchti,[55] V. I. Rud,[37] G. Sajot,[13] A. Sánchez-Hernández,[32] M. P. Sanders,[61] A. Santoro,[3] G. Savage,[50] L. Sawyer,[60] T. Scanlon,[43] D. Schaile,[24] R. D. Schamberger,[72] Y. Scheglov,[39] H. Schellman,[53] P. Schieferdecker,[24] C. Schmitt,[25] C. Schwanenberger,[44] A. Schwartzman,[68] R. Schwienhorst,[65] J. Sekaric,[49] S. Sengupta,[49] H. Severini,[75] E. Shabalina,[51] M. Shamim,[59] V. Shary,[17] A. A. Shchukin,[38] W. D. Shephard,[55] R. K. Shivpuri,[27] D. Shpakov,[50] V. Siccardi,[18] R. A. Sidwell,[59] V. Simak,[9] V. Sirotenko,[50] P. Skubic,[75] P. Slattery,[71] R. P. Smith,[50] G. R. Snow,[67] J. Snow,[74] S. Snyder,[73] S. Söldner-Rembold,[44] X. Song,[52] L. Sonnenschein,[16] A. Sopczak,[42] M. Sosebee,[78] K. Soustruznik,[8] M. Souza,[2] B. Spurlock,[78] J. Stark,[13] J. Steele,[60] V. Stolin,[36] A. Stone,[51] D. A. Stoyanova,[38] J. Strandberg,[64] S. Strandberg,[40] M. A. Strang,[69] M. Strauss,[75] R. Ströhmer,[24] D. Strom,[53] M. Strovink,[46] L. Stutte,[50] S. Sumowidagdo,[49] P. Svoisky,[55] A. Sznajder,[3] M. Talby,[14] P. Tamburello,[45] W. Taylor,[5] P. Telford,[44] J. Temple,[45] B. Tiller,[24] M. Titov,[22] V. V. Tokmenin,[35] M. Tomoto,[50] T. Toole,[61] I. Torchiani,[22] S. Towers,[42] T. Trefzger,[23] S. Trincaz-Duvoid,[16] D. Tsybychev,[72] B. Tuchming,[17] C. Tully,[68] A. S. Turcot,[44] P. M. Tuts,[70] R. Unalan,[65] L. Uvarov,[39] S. Uvarov,[39] S. Uzunyan,[52] B. Vachon,[5] P. J. van den Berg,[33] R. Van Kooten,[54] W. M. van Leeuwen,[33] N. Varelas,[51] E. W. Varnes,[45] A. Vartapetian,[78] I. A. Vasilyev,[38] M. Vaupel,[25] P. Verdier,[19] L. S. Vertogradov,[35] M. Verzocchi,[50] F. Villeneuve-Seguier,[43] P. Vint,[43] J.-R. Vlimant,[16] E. Von Toerne,[59] M. Voutilainen,[67,†] M. Vreeswijk,[33] H. D. Wahl,[49] L. Wang,[61] M. H. L. S Wang,[50] J. Warchol,[55] G. Watts,[82] M. Wayne,[55] G. Weber,[23] M. Weber,[50] H. Weerts,[65] N. Wermes,[21] M. Wetstein,[61] A. White,[78] D. Wicke,[25] G. W. Wilson,[58] S. J. Wimpenny,[48] M. Wobisch,[50] J. Womersley,[50] D. R. Wood,[63] T. R. Wyatt,[44] Y. Xie,[77] N. Xuan,[55] S. Yacoob,[53] R. Yamada,[50] M. Yan,[61] T. Yasuda,[50] Y. A. Yatsunenko,[35] K. Yip,[73] H. D. Yoo,[77] S. W. Youn,[53] C. Yu,[13] J. Yu,[78] A. Yurkewicz,[72] A. Zatserklyaniy,[52] C. Zeitnitz,[25] D. Zhang,[50] T. Zhao,[82] B. Zhou,[64] J. Zhu,[72] M. Zielinski,[71] D. Zieminska,[54] A. Zieminski,[54] V. Zutshi,[52] and E. G. Zverev[37]

(D0Collaboration)

[1]*Universidad de Buenos Aires, Buenos Aires, Argentina*
[2]*LAFEX, Centro Brasileiro de Pesquisas Físicas, Rio de Janeiro, Brazil*
[3]*Universidade do Estado do Rio de Janeiro, Rio de Janeiro, Brazil*
[4]*Instituto de Física Teórica, Universidade Estadual Paulista, São Paulo, Brazil*
[5]*University of Alberta, Edmonton, Alberta, Canada, Simon Fraser University, Burnaby, British Columbia, Canada,*
[6]*University of Science and Technology of China, Hefei, People's Republic of China*
[7]*Universidad de los Andes, Bogotá, Colombia*
[8]*Center for Particle Physics, Charles University, Prague, Czech Republic*
[9]*Czech Technical University, Prague, Czech Republic*
[10]*Center for Particle Physics, Institute of Physics, Academy of Sciences of the Czech Republic, Prague, Czech Republic*
[11]*Universidad San Francisco de Quito, Quito, Ecuador*
[12]*Laboratoire de Physique Corpusculaire, IN2P3-CNRS, Université Blaise Pascal, Clermont-Ferrand, France*
[13]*Laboratoire de Physique Subatomique et de Cosmologie, IN2P3-CNRS, Universite de Grenoble 1, Grenoble, France*
[14]*CPPM, IN2P3-CNRS, Université de la Méditerranée, Marseille, France*
[15]*IN2P3-CNRS, Laboratoire de l'Accélérateur Linéaire, Orsay, France*
[16]*LPNHE, IN2P3-CNRS, Universités Paris VI and VII, Paris, France*
[17]*DAPNIA/Service de Physique des Particules, CEA, Saclay, France*
[18]*IPHC, IN2P3-CNRS, Université Louis Pasteur, Strasbourg, France, and Université de Haute Alsace, Mulhouse, France*
[19]*Institut de Physique Nucléaire de Lyon, IN2P3-CNRS, Université Claude Bernard, Villeurbanne, France*
[20]*III. Physikalisches Institut A, RWTH Aachen, Aachen, Germany*
[21]*Physikalisches Institut, Universität Bonn, Bonn, Germany*
[22]*Physikalisches Institut, Universität Freiburg, Freiburg, Germany*
[23]*Institut für Physik, Universität Mainz, Mainz, Germany*
[24]*Ludwig-Maximilians-Universität München, München, Germany*
[25]*Fachbereich Physik, University of Wuppertal, Wuppertal, Germany*
[26]*Panjab University, Chandigarh, India*
[27]*Delhi University, Delhi, India*
[28]*Tata Institute of Fundamental Research, Mumbai, India*
[29]*University College Dublin, Dublin, Ireland*
[30]*Korea Detector Laboratory, Korea University, Seoul, Korea*

[31]*SungKyunKwan University, Suwon, Korea*
[32]*CINVESTAV, Mexico City, Mexico*
[33]*FOM-Institute NIKHEF and University of Amsterdam/NIKHEF, Amsterdam, The Netherlands*
[34]*Radboud University Nijmegen/NIKHEF, Nijmegen, The Netherlands*
[35]*Joint Institute for Nuclear Research, Dubna, Russia*
[36]*Institute for Theoretical and Experimental Physics, Moscow, Russia*
[37]*Moscow State University, Moscow, Russia*
[38]*Institute for High Energy Physics, Protvino, Russia*
[39]*Petersburg Nuclear Physics Institute, St. Petersburg, Russia*
[40]*Lund University, Lund, Sweden, Royal Institute of Technology*
and Stockholm University, Stockholm, Sweden, and Uppsala University, Uppsala, Sweden
[41]*Physik Institut der Universität Zürich, Zürich, Switzerland*
[42]*Lancaster University, Lancaster, United Kingdom*
[43]*Imperial College, London, United Kingdom*
[44]*University of Manchester, Manchester, United Kingdom*
[45]*University of Arizona, Tucson, Arizona 85721, USA*
[46]*Lawrence Berkeley National Laboratory and University of California, Berkeley, California 94720, USA*
[47]*California State University, Fresno, California 93740, USA*
[48]*University of California, Riverside, California 92521, USA*
[49]*Florida State University, Tallahassee, Florida 32306, USA*
[50]*Fermi National Accelerator Laboratory, Batavia, Illinois 60510, USA*
[51]*University of Illinois at Chicago, Chicago, Illinois 60607, USA*
[52]*Northern Illinois University, DeKalb, Illinois 60115, USA*
[53]*Northwestern University, Evanston, Illinois 60208, USA*
[54]*Indiana University, Bloomington, Indiana 47405, USA*
[55]*University of Notre Dame, Notre Dame, Indiana 46556, USA*
[56]*Purdue University Calumet, Hammond, Indiana 46323, USA*
[57]*Iowa State University, Ames, Iowa 50011, USA*
[58]*University of Kansas, Lawrence, Kansas 66045, USA*
[59]*Kansas State University, Manhattan, Kansas 66506, USA*
[60]*Louisiana Tech University, Ruston, Louisiana 71272, USA*
[61]*University of Maryland, College Park, Maryland 20742, USA*
[62]*Boston University, Boston, Massachusetts 02215, USA*
[63]*Northeastern University, Boston, Massachusetts 02115, USA*
[64]*University of Michigan, Ann Arbor, Michigan 48109, USA*
[65]*Michigan State University, East Lansing, Michigan 48824, USA*
[66]*University of Mississippi, University, Mississippi 38677, USA*
[67]*University of Nebraska, Lincoln, Nebraska 68588, USA*
[68]*Princeton University, Princeton, New Jersey 08544, USA*
[69]*State University of New York, Buffalo, New York 14260, USA*
[70]*Columbia University, New York, New York 10027, USA*
[71]*University of Rochester, Rochester, New York 14627, USA*
[72]*State University of New York, Stony Brook, New York 11794, USA*
[73]*Brookhaven National Laboratory, Upton, New York 11973, USA*
[74]*Langston University, Langston, Oklahoma 73050, USA*
[75]*University of Oklahoma, Norman, Oklahoma 73019, USA*
[76]*Oklahoma State University, Stillwater, Oklahoma 74078, USA*
[77]*Brown University, Providence, Rhode Island 02912, USA*
[78]*University of Texas, Arlington, Texas 76019, USA*
[79]*Southern Methodist University, Dallas, Texas 75275, USA*
[80]*Rice University, Houston, Texas 77005, USA*
[81]*University of Virginia, Charlottesville, Virginia 22901, USA*
[82]*University of Washington, Seattle, Washington 98195, USA*

We measure the dimuon charge asymmetry A in $p\bar{p}$ collisions at a center of mass energy $\sqrt{s} = $ 1960 GeV. The data was recorded with the D0 detector and corresponds to an integrated luminosity of approximately 1.0 fb^{-1}. Assuming that the asymmetry A is due to asymmetric $B^0 \leftrightarrow \bar{B}^0$ mixing and

*On leave from IEP SAS Košice, Slovakia.
†Visitor from Helsinki Institute of Physics, Helsinki, Finland.

decay, we extract the *CP*-violation parameter of B^0 mixing and decay: $\frac{\Re(\epsilon_{B^0})}{1+|\epsilon_{B^0}|^2} = \frac{A_{B^0}}{4} = -0.0023 \pm 0.0011(\text{stat}) \pm 0.0008(\text{syst})$. A_{B^0} is the dimuon charge asymmetry from decays of $B^0\bar{B}^0$ pairs. The general case, with *CP* violation in both B^0 and B_s^0 systems, is also considered. Finally we obtain the forward-backward asymmetry that quantifies the tendency of μ^+ to go in the proton direction and μ^- to go in the antiproton direction. The results are consistent with the standard model and constrain new physics.

I. INTRODUCTION

We measure the dimuon charge asymmetry:

$$A = \frac{N^{++} - N^{--}}{N^{++} + N^{--}} \quad (1)$$

in $p\bar{p}$ collisions at a center of mass energy $\sqrt{s} = 1960$ GeV. N^{++} (N^{--}) is the number of events with two positive (negative) muon candidates passing selection cuts. The data was recorded with the D0 detector at the Fermilab Tevatron between 2002 and 2005. The exposed integrated luminosity is approximately 1.0 fb^{-1}. Assuming that the asymmetry A is due to asymmetric $B^0 \leftrightarrow \bar{B}^0$ mixing and decay, we extract the *CP*-violation parameter of B^0 mixing and decay [1–3]:

$$\frac{\Re(\epsilon_{B^0})}{1+|\epsilon_{B^0}|^2} = \Im\left\{\frac{\Gamma_{12}}{4M_{12}}\right\} = \frac{A_{B^0}}{4} \equiv f \cdot A. \quad (2)$$

M_{12} (Γ_{12}) is the real (imaginary) part of the transition matrix element of the Hamiltonian corresponding to $(B^0, \bar{B}^0)$ mixing and decay. Throughout this article we use the Particle Data Group [1] notation: $B^0 = d\bar{b}$, $B_s^0 = s\bar{b}$. A_{B^0} is the dimuon charge asymmetry from direct-direct decays of $B^0\bar{B}^0$ (we define "direct decay" as $b \to \mu^- X$, and "sequential decay" as $b \to c \to \mu^+ X$). The dimuon charge asymmetry A in Eq. (2) excludes events with a muon from $K^\pm$ decay. Equation (2) defines the factor f, to be obtained below, which accounts for other processes contributing to dimuon events. As a sensitive cross check, we also measure the mean mixing probability χ_0 of $B \leftrightarrow \bar{B}$ hadrons, averaged over the mix of hadrons with a b quark. Finally we obtain the forward-backward asymmetry that quantifies the tendency of μ^+ to go in the proton direction and μ^- to go in the antiproton direction.

The general case, with *CP* violation in both B^0 and B_s^0 systems, is considered in the last section of this article. In this general case, the dimuon charge asymmetry A has contributions from both B^0 and B_s^0. Therefore, this measurement at the Fermilab Tevatron $p\bar{p}$ collider is complementary to similar measurements at B factories that are sensitive only to A_{B^0}, not $A_{B_s^0}$.

The CP-violation parameter, defined in Eq. (2), is sensitive to several extensions of the standard model because new particles may contribute to the box diagrams of M_{12} [3,4]. Reference [3] concludes that "It is possible that the dilepton asymmetry could be one of the first indications of physics beyond the standard model".

The D0 detector has an excellent muon system in Run II [5], with large (η, ϕ) coverage, good scintillator-based triggering and cosmic ray rejection, low punch-through rate, and precision tracking. The muon is the particle with cleanest identification. The like-sign dimuon channel is particularly clean: few processes contribute to it and fewer still contribute to an asymmetry. The D0 detector is well suited for this precision measurement.

The outline of the paper is as follows. The D0 detector is described in Sec. II. In Sec. III we consider the event selection. Physics and detector asymmetries are studied in Sec. IV. The processes contributing to the asymmetry A are presented in Section V, and their weights are summarized in Sec. VI. The breakdown of systematic uncertainties of A is discussed in Sec. VII. Cross-checks are listed in Sec. VIII. Final results are summarized in Sec. IX.

II. THE D0 DETECTOR

The D0 detector consists of a magnetic central-tracking system, comprised of a silicon microstrip tracker (SMT) and a central fiber tracker (CFT), both located within a 2 T superconducting solenoidal magnet [6]. The SMT has $\approx$ 800 000 individual strips, with typical pitch of 50–80 μm, and a design optimized for tracking and vertexing capability at pseudorapidities of $|\eta| < 2.5$. The system has a six-barrel longitudinal structure, each with a set of four layers arranged axially around the beam pipe, and interspersed with 16 radial disks. The CFT has eight thin coaxial barrels, each supporting two doublets of overlapping scintillating fibers of 0.835 mm diameter, one doublet being parallel to the collision axis, and the other alternating by $\pm 3°$ relative to the axis. Light signals are transferred via clear fibers to solid-state photon counters (VLPC) that have $\approx 80\%$ quantum efficiency.

Central and forward preshower detectors located just outside of the superconducting coil (in front of the calorimetry) are constructed of several layers of extruded triangular scintillator strips that are read out using wavelength-shifting fibers and VLPCs. The next layer of detection involves three liquid-argon/uranium calorimeters: a central section (CC) covering $|\eta|$ up to ≈ 1.1, and two endcap calorimeters (EC) that extend coverage to $|\eta| \approx 4.2$, all housed in separate cryostats [7]. In addition to the preshower detectors, scintillators between the CC and EC cryostats provide sampling of developing showers at $1.1 < |\eta| < 1.4$.

A muon system [5] is located beyond the calorimetry, and consists of a layer A of tracking detectors and scintillation trigger counters before 1.8 T iron toroids, followed by two similar layers B and C after the toroids. Tracking at $|\eta| < 1$ relies on 10 cm wide drift tubes [7], while 1 cm mini-drift tubes are used at $1 < |\eta| < 2$. Layer A is subdivided into one plane of scintillation trigger counters and 4 planes of drift tubes. Layers B and C are each subdivided into one plane of scintillation trigger counters and 3 planes of drift tubes.

A muon originating in a $p\bar{p}$ collision traverses the silicon microstrip tracker and the scintillating fiber tracker in the 2 T solenoidal magnetic field, the calorimeter, layer A of the muon spectrometer, the 1.8 T magnetized iron toroid, and layers B and C of the spectrometer. The momentum of the muon is measured twice: once by the local muon system comprised of layers A, B and C, and once by the central-tracking system.

Luminosity is measured using plastic scintillator arrays located in front of the EC cryostats, covering $2.7 < |\eta| < 4.4$.

Trigger and data acquisition systems are designed to accommodate the high luminosities of Run II. Based on preliminary information from tracking, calorimetry, and muon systems, the output of the first level of the trigger is used to limit the rate for accepted events to ≈ 2 kHz. At the next trigger stage, with more refined information, the rate is reduced further to ≈ 1 kHz. These first two levels of triggering rely mainly on hardware and firmware. The third and final level of the trigger, with access to all the event information, uses software algorithms and a computing farm, and reduces the output rate to ≈ 50 Hz, which is written to tape.

The polarities of the toroid and solenoid magnetic fields are reversed roughly every two weeks so that the four solenoid-toroid polarity combinations are exposed to approximately the same integrated luminosity. This allows cancellation of first-order effects of the detector geometry.

III. EVENT SELECTION

Our standard cuts require global muons, i.e., local muon candidates (reconstructed from hits in layers A, B and C) with a matching central track (reconstructed from hits in the silicon and fiber trackers). To reduce punch-through of hadrons we only consider muons that traverse the iron toroid. To select muons that emerge from the toroid with momentum $p \gtrsim 0.2$ GeV/c, we require *either* $p_T > 4.2$ GeV/c *or* $|p_z| > 6.4$ GeV/c, where p_T is the momentum transverse to the beam measured by the central-tracking system, and p_z is the component of the momentum in the direction of the proton beam. See the geometry of the iron toroids in Fig. 1. We require at least two wire chamber hits in the A layer and at least three wire chamber hits in layers B or C. We require local and global track fits with good χ^2. To reduce cosmic ray background, we
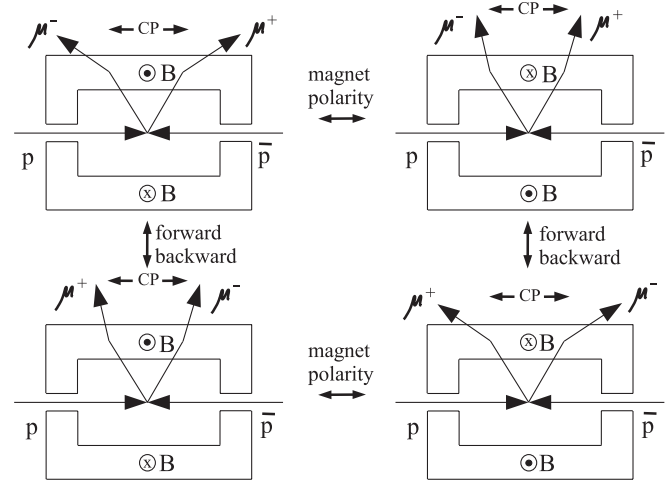
FIG. 1. Schematic drawing of the magnetized iron toroids of the D0 detector, and muon tracks related by toroid polarity reversal, *CP* conjugation and forward-backward reflection.

require at least one scintillator hit associated with the muon to be within a time window of ± 5 ns with respect to the expected time. To reduce muons from $K^{\pm}$ and $\pi^{\pm}$ decay, we require $p_T > 3.0$ GeV/c. The track is required to have a distance of closest approach to the beam less than 0.3 cm. We use the full pseudorapidity range $|\eta| < 2.2$. We apply a cut of $p_T < 15.0$ GeV/c to reduce the number of muons reconstructed with wrong sign, and to reduce the background from $W^{\pm}$ and Z boson decay. This list completes the single muon cuts.

The dimuon cuts are as follows. We require that both muon candidates pass within 2.0 cm of each other in the direction along the beam line at the point of closest approach to the beam. To further reduce cosmic rays and repeated reconstructions of the same track (with different hits), we require the 3-dimensional opening angle between the muons to be between 10° and 170°. We also require that the two muons have different A layer positions (by at least 5 cm), different local momentum vectors (by at least 0.2 GeV/c), and different central track momentum vectors (by at least 0.2 GeV/c). This completes the set of standard cuts.

To avoid a bias due to mismatched central tracks (which are measured to be charge-asymmetric) we use the local muon charge, instead of the matching central track charge, to obtain the asymmetries. The positive charge asymmetry of central tracks is due to secondary particles that emerge from interactions with detector material. The measured charge asymmetry of central tracks with $p_T > 3.0$ GeV/c is $(N^+ - N^-)/(N^+ + N^-) = 0.0049 \pm 0.0005$.

The measurement of the dimuon charge asymmetry *A* is based on *ratios of muon counts*. To minimize the statistical error we use all recorded events regardless of trigger. If an event passes cuts, it is valid to accept it regardless of trigger, since an event with opposite muon charges can also be accepted by that trigger.
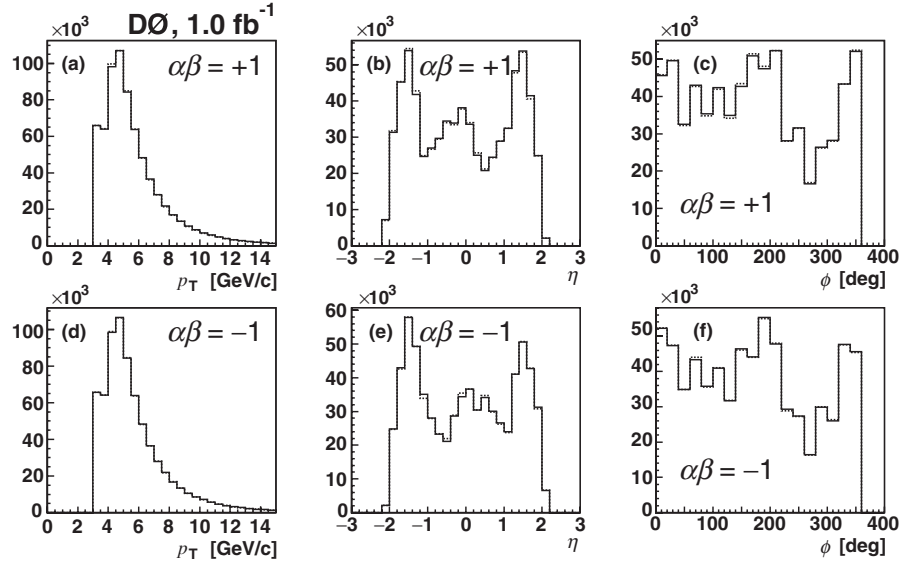
FIG. 2.   Distributions of single muon p_T (a) and (d), η (b) and (e), and ϕ (c) and (f), for events with opposite toroid and solenoid polarities passing standard single muon and dimuon cuts. The charge times toroid polarity, $\alpha\beta$, is indicated in the labels. Each plot superposes two histograms with opposite charge and opposite polarities. Positive (negative) charge corresponds to solid (dotted) lines (that can generally not be distinguished). Histograms with negative toroid polarity are scaled by the ratio of muon counts $e = 1.0300$, see Sec. IV.

Histograms of p_T, η, and ϕ for standard cuts are shown in Figs. 2 and 3. Each plot superposes two histograms with opposite charge and opposite polarities (that can generally not be distinguished).

IV. ASYMMETRIES

In this Section we study detector and physics effects that may alter the charge asymmetry and therefore contribute to corrections and systematic uncertainties. The muon detec-

tor is shown schematically in Fig. 1. How can the detector introduce a charge asymmetry? It would have to have different acceptance × efficiency for positive and negative muons, i.e., for tracks bending north and south in the magnetized iron toroid, see Fig. 1. Such a difference may be due to an offset of the mean beam spot, to mechanical asymmetries, and to differences in wire chamber and scintillator efficiencies. We find that the detector, operating with a given toroid and solenoid polarity, introduces an apparent dimuon charge asymmetry of approximately
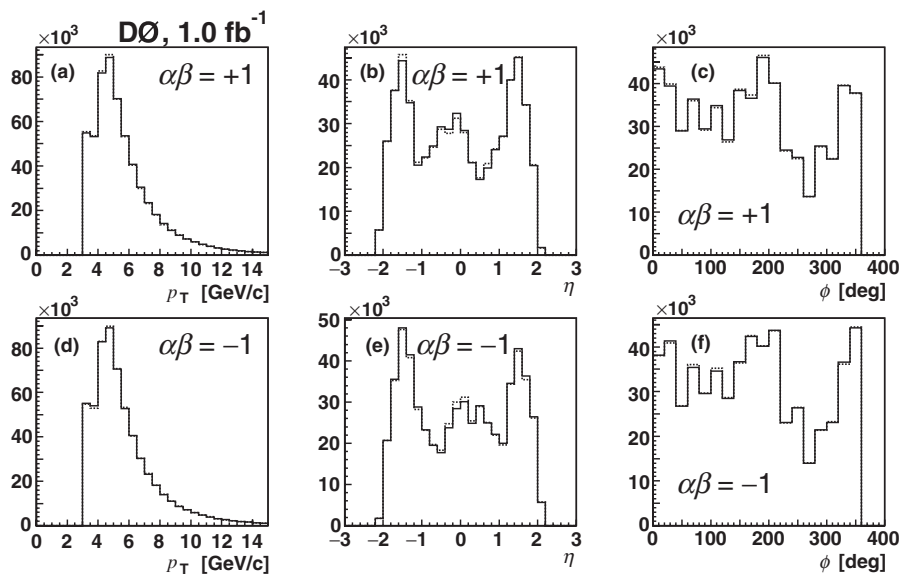
FIG. 3.   Same as Fig. 2, but for equal toroid and solenoid polarities. Here $e = 0.9292$.

0.006 in absolute value (to be discussed later in this Section). This detector effect changes sign when the toroid and solenoid polarities are reversed (since the exact same track that is called "positive" with one polarity is called "negative" with the opposite polarity). This effect can be seen by comparing the η histograms in Figs. 2 and 3. Therefore, to cancel detector geometry effects to first order, we always consider data sets that have equal event counts for each toroid-solenoid magnet polarity (or weight the events appropriately). We combine events with one solenoid polarity and toroid polarity, with events with the opposite solenoid polarity and toroid polarity. The analysis is done separately for solenoid polarity equal to the toroid polarity, and solenoid polarity opposite to the toroid polarity.

Let $n_\alpha^{\beta\gamma}$ be the number of muons passing cuts with charge $\alpha = \pm 1$, toroid polarity $\beta = \pm 1$, and $\gamma = +1$ if $\eta > 0$ and $\gamma = -1$ if $\eta < 0$.

We model the physics and the detector as follows:

$$n_\alpha^{\beta\gamma} \equiv \frac{1}{4} N \epsilon^\beta (1 + \alpha A)(1 + \alpha\gamma A_{\mathrm{fb}})(1 + \gamma A_{\mathrm{det}})$$
$$\times (1 + \alpha\beta\gamma A_{\mathrm{ro}})(1 + \beta\gamma A_{\beta\gamma})(1 + \alpha\beta A_{\alpha\beta}), \quad (3)$$

where $\epsilon^+ + \epsilon^- = 1$. The eight Eqs. (3) *define* eight parameters in terms of the eight numbers $n_\alpha^{\beta\gamma}$. The parameters are N, $\epsilon^+$, and six asymmetries. $N\epsilon^\beta$ is approximately equal to the number of muons passing cuts with toroid polarity β. A is the dimuon charge asymmetry, A_{fb} is the forward-backward asymmetry (that quantifies the tendency of μ^+ to go in the proton direction and μ^- to go in the antiproton direction), A_{det} measures the north-south asymmetry of the detector ("north" has $\eta < 0$), and A_{ro} is the range-out asymmetry (that quantifies the change in acceptance and range-out of muon tracks that bend toward, or away from, the beam line, see Fig. 1). $A_{\alpha\beta}$ is a detector asymmetry between tracks bending north and tracks bending south. A and A_{fb} are physics asymmetries that we want to measure, and A_{det}, A_{ro} and $A_{\alpha\beta}$ are detector asymmetries. $A_{\beta\gamma}$ is a second-order asymmetry that is different from zero only if A *and* A_{ro} are different from zero. If the selection of events includes single muon *and* dimuon cuts, we use capital A for the asymmetries. If only single muon cuts are required, we use lower case a. In Tables I and II we show the numbers $n_\alpha^{\beta\gamma}$ for our standard cuts. The measured asymmetries are presented in Table III.

We can understand the detector asymmetry $A_{\alpha\beta}$ in more detail. Let A^β be the dimuon charge asymmetry of events with toroid polarity β. From Eq. (3) we obtain, to first order in the asymmetries, $A^\beta = A + \beta A_{\alpha\beta}$. Therefore $\beta A_{\alpha\beta}$ is the dimuon charge asymmetry due to detector geometry effects. It changes sign when the magnet polarities are reversed. This is the detector geometry effect that is cancelled by taking the weighted average of A^+ and A^-.

TABLE I. Numbers $n_\alpha^{\beta\gamma}$ of muons passing standard single and dimuon cuts with charge α, toroid magnet polarity β, and $\eta < 0$ ($\gamma = -1$) or >0 ($\gamma = +1$). There are two entries per event. The solenoid and toroid polarities are opposite. In total there are 154667 positive-positive, 154482 negative-negative, and 1075192 positive-negative dimuon events. No cuts on the dimuon mass are imposed at this stage.

charge	toroid	$-2.2 < \eta < 0.0$	$0.0 < \eta < 2.2$
α	polarity β	$\gamma = -1$	$\gamma = +1$
$+1$	$+1$	367376	335700
-1	$+1$	348295	353453
$+1$	-1	337697	343753
-1	-1	356891	325517

The magnitude of this effect is $A_{\alpha\beta} \approx -0.006$, see Table III.

Solving Eqs. (3) up to second-order terms in the asymmetries, A is obtained by taking the weighted average $\frac{1}{2} \times (A^+ + eA^-)$:

$$\frac{(n_+^{++} + n_+^{+-} - n_-^{++} - n_-^{+-}) + e(n_+^{-+} + n_+^{--} - n_-^{-+} - n_-^{--})}{(n_+^{++} + n_+^{+-} + n_-^{++} + n_-^{+-}) + e(n_+^{-+} + n_+^{--} + n_-^{-+} + n_-^{--})}$$
$$= A + A_{\mathrm{fb}}A_{\mathrm{det}}, \quad (4)$$

where $e \equiv \epsilon^+/\epsilon^-$. To the required accuracy, e is the ratio of the number of events passing cuts with toroid polarity $\beta = +1$ over the corresponding number with $\beta = -1$. The ratio e is determined by counting single muons for the single muon asymmetries, or by counting dimuons for the dimuon analysis. This procedure introduces no bias since we count all muons or dimuons regardless of the charges of each muon. The left-hand-side is the measured asymmetry, A is the corrected asymmetry, and $-A_{\mathrm{fb}}A_{\mathrm{det}}$ is the correction due to the forward-backward *and* detector asymmetries. We do not apply this correction because it turns out to be negligible and compatible with zero, see Table III. We use the correction to estimate the corresponding systematic uncertainty. We can understand the last term in Eq. (4): if positive (negative) muons prefer to go in the proton (antiproton) direction *and* the detector is north-south asymmetric, then we obtain an apparent charge asymmetry.

TABLE II. Same as Table I, but for equal solenoid and toroid polarities. In total there are 136422 positive-positive, 136857 negative-negative, and 944013 positive-negative dimuon events.

charge	toroid	$-2.2 < \eta < 0.0$	$0.0 < \eta < 2.2$
α	polarity β	$\gamma = -1$	$\gamma = +1$
$+1$	$+1$	306594	279508
-1	$+1$	290270	296264
$+1$	-1	311153	319602
-1	-1	329285	301908

TABLE III. Asymmetries described in Sec. IV are shown for central (c) muons, $|\eta| < 0.95$, and forward (f) muons, $0.95 < |\eta| < 2.2$. All errors are statistical. The average for opposite and equal toroid and solenoid polarities (torpol · solpol = −1 and 1) is $A = -0.0005 \pm 0.0013$ (all).

torpol*solpol	−1	1
e	1.0300	0.9292
a (all)	0.0001 ± 0.0005	-0.0012 ± 0.0005
a_{fb} (all)	0.0021 ± 0.0005	0.0011 ± 0.0005
a_{det} (all)	-0.0074 ± 0.0005	-0.0045 ± 0.0005
a_{ro} (all)	-0.0268 ± 0.0005	-0.0298 ± 0.0005
a (c)	-0.0014 ± 0.0007	-0.0035 ± 0.0008
a_{fb} (c)	0.0004 ± 0.0007	-0.0010 ± 0.0008
a_{det} (c)	-0.0069 ± 0.0007	-0.0068 ± 0.0008
a_{ro} (c)	-0.0867 ± 0.0007	-0.0891 ± 0.0008
a (f)	0.0010 ± 0.0006	0.0003 ± 0.0006
a_{fb} (f)	0.0033 ± 0.0006	0.0025 ± 0.0006
a_{det} (f)	-0.0078 ± 0.0006	-0.0029 ± 0.0006
a_{ro} (f)	0.0122 ± 0.0006	0.0089 ± 0.0006
A_{fb} (all)	0.0006 ± 0.0006	0.0001 ± 0.0007
A_{det} (all)	-0.0187 ± 0.0006	-0.0165 ± 0.0007
A_{ro} (all)	-0.0268 ± 0.0006	-0.0283 ± 0.0007
$A_{\alpha\beta}$ (all)	-0.0059 ± 0.0006	-0.0069 ± 0.0007
$A_{\beta\gamma}$ (all)	-0.0002 ± 0.0006	-0.0015 ± 0.0007
R	0.4603 ± 0.0013	0.4610 ± 0.0013
A_{fc} (all)	-0.0008 ± 0.0026	-0.0023 ± 0.0027
A_{fe} (all)	0.0019 ± 0.0026	-0.0008 ± 0.0028
A (cc)	0.0015 ± 0.0044	-0.0021 ± 0.0048
A (ff)	0.0024 ± 0.0031	0.0016 ± 0.0033
A (all)	0.0005 ± 0.0018	-0.0016 ± 0.0019

The forward-backward asymmetry A_{fb} (up to second-order terms) is:

$$\frac{(n_+^{++} + n_-^{+-} - n_+^{+-} - n_-^{++}) + e(n_+^{-+} + n_-^{--} - n_+^{--} - n_-^{-+})}{(n_+^{++} + n_-^{+-} + n_+^{+-} + n_-^{++}) + e(n_+^{-+} + n_-^{--} + n_+^{--} + n_-^{-+})}$$
$$= A_{\mathrm{fb}} + A A_{\mathrm{det}}. \tag{5}$$

We have repeated the study of detector asymmetries for the central ($|\eta| < 0.95$) and forward ($0.95 < |\eta| < 2.2$) muon systems separately.

Also shown in Table III is the dimuon charge asymmetry for flavor creation A_{fc} (defined as $\Delta\psi \geq 90°$) and flavor excitation A_{fe} (defined as $\Delta\psi < 90°$), where $\Delta\psi$ is the 3-dimensional angle between the two muons. Flavor creation corresponds to the b and $\bar{b}$ quarks in opposite jets, while flavor excitation corresponds generally to a $b\bar{b}$ pair produced in the hadronization of one parton, including gluon splitting. The accepted cross sections for flavor creation and flavor excitation are nearly equal (as indicated by their statistical errors in Table III). In Table III we also show the ratio $R = (N^{++} + N^{--})/N^{+-}$ of like-sign to opposite-sign dimuon events in either the mass window 5.0 to 8.7 GeV/c^2 or 11.5 to 30 GeV/c^2 for events passing a

dimuon trigger. This ratio is used for mixing studies. These mass windows reduce backgrounds from same-side direct-sequential muon pairs (process P_4 in Table IV), and decays of J/ψ's, Υ's and their resonances (part of process P_6), defined later.

V. DIMUON PROCESSES

In this Section we obtain the factor f defined in Eq. (2). We consider the processes P_1–P_{13} listed in Table IV. P_1 is direct-direct $b\bar{b}$ decay. P_2 is opposite-side direct-sequential decay. P_3 is sequential-sequential decay. P_4 is same-side direct-sequential decay. P_7 corresponds to cosmic ray muons that traverse the D0 detector and are reconstructed twice: once upon entry and once upon exit. P_8 corresponds to muons from $K^\pm$ decay, in coincidence with a prompt muon from the collision. This process is discussed in detail in Secs. VI and VII. P_9 corresponds to a cosmic ray muon, in coincidence with a prompt muon. P_{10} corresponds to a hadron that traverses the calorimeter and iron toroid and is reconstructed as a muon, in coincidence with a prompt muon. P_{11} corresponds to a combinatoric background faking a muon, in coincidence with a prompt muon. Examples of "other" processes P_{12} are dimuons with the following parents: $B^\pm$ and $\pi^\pm$, $\bar{B}^0$ and $\tau^\pm$, B_s^0 and J/ψ, B^0 and $\tau^\pm$, $\bar{B}^0$ and J/ψ, $B^\pm$ and $\tau^\pm$, b and unrelated c. P_{13} are events that have one of the muons reconstructed with the wrong sign. Contributions from both muons coming from hadron misidentification or combinatoric background are negligible.

Let χ_d be the probability that a $\bar{B}^0(b\bar{d})$ meson that decays to a flavor specific final state, mixes and decays as a $B^0(d\bar{b})$. Similarly, $\bar{\chi}_d$ is the probability that a B^0 meson mixes and decays as a $\bar{B}^0$. Here we consider the possibility that $\chi_d \neq \bar{\chi}_d$ (the general case with $\chi_d \neq \bar{\chi}_d$ and $\chi_s \neq \bar{\chi}_s$ is considered in Sec. IX). The probability that a b quark in the sample decays as a $\bar{b}$ is

$$\chi = f_d \frac{\beta_d}{\langle\beta\rangle}\chi_d + f_s \frac{\beta_s}{\langle\beta\rangle}\chi_s, \tag{6}$$

where f_d and f_s are the fractions of b quarks that hadronize to B^0 or $\bar{B}^0$ and B_s^0 or $\bar{B}_s^0$ respectively, and β_d, β_s and $\langle\beta\rangle$ are the branching fractions for B^0, B_s^0 and the b-hadron admixture, respectively, decaying to μX with μ passing cuts. Similarly,

$$\bar{\chi} = f_d \frac{\beta_d}{\langle\beta\rangle}\bar{\chi}_d + f_s \frac{\beta_s}{\langle\beta\rangle}\chi_s \tag{7}$$

is the probability that a $\bar{b}$ in the sample decays as a b. From Ref. [1] we take $f_d = 0.397 \pm 0.010$, $f_s = 0.107 \pm 0.011$, $\chi_{d0} \equiv \frac{1}{2}(\chi_d + \bar{\chi}_d) = 0.186 \pm 0.004$, and $\chi_{s0} \equiv \frac{1}{2} \times (\chi_s + \bar{\chi}_s) > 0.49883$. We take $\beta_d = \beta_s = \langle\beta\rangle$. To abbreviate, we define $\chi_0 \equiv \frac{1}{2}(\chi + \bar{\chi})$, and $\xi \equiv 2\chi_0(1 - \chi_0)$. We assume *CPT* symmetry. The probability that a B ($\bar{B}$) hadron that decays to a flavor specific final state, decays as a B ($\bar{B}$) is then $1 - \chi_0$. From Table IV we obtain the

TABLE IV. Processes contributing to dimuon events. Each row includes processes related by *CP* conjugation and $B \leftrightarrow \bar{B}$ mixing. The weights are normalized to direct-direct $b\bar{b}$ decay $P_1 \equiv 1$. $\xi \equiv 2\chi_0(1 - \chi_0)$. $\chi = f_d\chi_d + f_s\chi_s$ is the probability that b quarks decay as $\bar{b}$. $\bar{\chi} = f_d\bar{\chi}_d + f_s\chi_s$ is the probability that $\bar{b}$ antiquarks decay as b. The fraction of prompt muons from b decay is $\rho' \equiv 0.6 \pm 0.15$ [8]. $\rho \equiv \frac{1}{2}\rho'(\chi - \bar{\chi})$. $a = 0.026 \pm 0.005$ is the charge asymmetry of $K^\pm$ decay, see the text. *CPT* symmetry is assumed. For example, the number of direct-direct decays $b\bar{b} \to \mu^+\mu^+X$ is $\propto P_1\chi(1 - \chi_0)$.

process	weight	N^{++}	N^{--}	N^{+-}
$b \to \mu^-, \bar{b} \to \mu^+$	$P_1 \equiv 1$	$\chi(1 - \chi_0)$	$(1 - \chi_0)\bar{\chi}$	$1 - \xi$
$b \to \mu^-, \bar{b} \to \bar{c} \to \mu^-$	P_2	$\frac{1}{2}(1 - \xi)$	$\frac{1}{2}(1 - \xi)$	ξ
$b \to c \to \mu^+, \bar{b} \to \bar{c} \to \mu^-$	P_3	$(1 - \chi_0)\bar{\chi}$	$\chi(1 - \chi_0)$	$1 - \xi$
$b \to \mu^- c \to \mu^+$	P_4	0	0	1
$c \to \mu^+, \bar{c} \to \mu^-$	P_5	0	0	1
Drell-Yan, J/ψ, Υ	P_6	0	0	1
dimuon cosmic rays	P_7	≈ 0.14	≈ 0.14	≈ 0.72
$\mu + K^\pm$ decay	P_8	$0.25 \cdot (1 + a + \rho)$	$0.25 \cdot (1 - a - \rho)$	0.5
$\mu + $ cosmic	P_9	$\approx 0.25 \cdot (1 + \rho)$	$\approx 0.25 \cdot (1 - \rho)$	≈ 0.5
$\mu + $ punch-through	P_{10}	$0.25 \cdot (1 + \rho)$	$0.25 \cdot (1 - \rho)$	0.5
$\mu + $ combinatoric	P_{11}	$0.25 \cdot (1 + \rho)$	$0.25 \cdot (1 - \rho)$	0.5
other	P_{12}	$0.25 \cdot (1 + \rho)$	$0.25 \cdot (1 - \rho)$	0.5
dimuon w. wrong sign	P_{13}	0.39	0.39	0.22

dimuon charge asymmetry A after correcting for asymmetric kaon decay, (i.e., after subtracting a term $0.5aP_8$ in the numerator),

$$A = \frac{(\chi - \bar{\chi})[(1 - \chi_0)(P_1 - P_3) + 0.25\rho'P_8']}{A_{\text{den}}}, \quad (8)$$

and the factor f in Eq. (2):

$$f = \frac{A_{\text{den}}}{8f_d\chi_{d0}[(1 - \chi_0)(P_1 - P_3) + 0.25\rho'P_8']}, \quad (9)$$

where $A_{\text{den}} = \xi(P_1 + P_3) + (1 - \xi)P_2 + 0.28P_7 + 0.5P_8' + 0.78P_{13}$ and $P_8' \equiv P_8 + P_9 + P_{10} + P_{11} + P_{12}$. The fraction of prompt muons from b decay is $\rho' \equiv 0.6 \pm 0.15$ [8].

VI. WEIGHTS P_i OF DIMUON PROCESSES

The weights P_2 through P_{13}, normalized to direct-direct $b\bar{b}$ decay $P_1 \equiv 1$, are summarized in Table V. The weights P_2, P_4, P_5, P_6 and P_{12} were obtained from Monte Carlo simulations (using the PYTHIA generator [9]) with full detector simulation (based on the GEANT program [10]) and event reconstruction and selection. A cross-check for weight P_2 is the measurement of the average mixing probability of B hadrons to be described below. Weights P_4, P_5 and P_6 do not contribute like-sign dimuons, and so do not enter into the measurement of the *CP*-violation parameter. Weight P_3 was obtained from $P_3 \approx P_2^2/(4P_1)$. Weight P_7 was obtained by two methods: (i) from the data of a cosmic ray run, and (ii) extrapolating the out-of-time muon background (as measured by the scintillators) into the acceptance window of ± 5 ns. Weight P_9 was obtained using the data of the cosmic ray run. Weight P_{10} was obtained by counting the number of tracks that had enough

momentum to traverse the calorimeter and iron toroid, and multiplying by the probability $\exp(-14)$ that they do not interact (the calorimeter has ≈ 7 nuclear interaction lengths, and the iron toroid has ≈ 7 nuclear interaction lengths). Weight P_{11} was estimated by relaxing the number of required wire chamber hits (one less hit in layer A and/or 1 less hit in layers B or C). Weight P_{13} was estimated using the measured resolution of the local muon spectrometer. In our data set, passing standard single and dimuon cuts, we expect ≈ 1 dimuon event from Z boson decay, and less than one event from prompt muons plus $W^\pm$ boson decay.

Let us consider the weight P_8 in some detail. This weight corresponds to prompt muons from b or c or s decay plus $K^\pm$ decay. This is an important background because kaon interactions are charge asymmetric, and dominate the systematic uncertainty of the measurement

TABLE V. Weights of dimuon processes for standard cuts (obtained as described in the text). Note that 64% of dimuons are from direct-direct $b\bar{b}$ decay.

P_1	$\equiv 1$
P_2	0.116 ± 0.055
P_3	0.003 ± 0.003
P_4	0.093 ± 0.049
P_5	0.070 ± 0.042
P_6	0.023 ± 0.023
P_7	0.003 ± 0.003
P_8	0.078 ± 0.023
P_9	0.0001 ± 0.0001
P_{10}	0.001 ± 0.001
P_{11}	0.0002 ± 0.0002
P_{12}	0.163 ± 0.066
P_{13}	0.0005 ± 0.0005

of the *CP*-violation parameter. The inelastic interaction length of K^+ in the calorimeter is greater than the inelastic interaction length of K^-. This difference is due to the existence of hyperons Y (strangeness -1 baryons: Λ, Σ, Y^*). Reactions $K^- N \rightarrow Y\pi$ have no $K^+ N$ analog. Therefore K^+ has more time to decay than K^-. The result is a charge asymmetry from $K^\pm$ decay. The single muon charge asymmetry from $K^\pm$ decay is obtained from the inelastic cross sections for $K^- d$ and $K^+ d$ [1] and the geometry and materials of the D0 detector: $a \equiv (n^+ - n^-)/(n^+ + n^-) = 0.026 \pm 0.005$.

For P_8, we make two complementary estimates based on data. In the first, we measure the exclusive decay $B^0 \rightarrow D^*(2010)^- \mu^+ \nu_\mu$, $D^*(2010)^- \rightarrow \bar{D}^0 \pi^-$, $\bar{D}^0 \rightarrow K^+ \pi^-$, and its charge conjugate. We apply standard single and dimuon cuts, and count events with and without a muon matching the kaon track. We subtract the background by two methods: using a side-band of $m_{D^{*-}} - m_{D^0}$, or using the wrong relative sign of the muon from B^0 decay and the pion from D^{*-} decay. The result is $P_8 = 0.078 \pm 0.013(\text{stat}) \pm 0.019(\text{syst})$. From studies with this exclusive decay, we learn that the global track χ^2-cut is not very effective in reducing $K^\pm$ decay kinks (for the high momentum muons passing cuts). Therefore we must correct A for $K^\pm$ decay as discussed in Sec. VII.

We use the following alternative procedure to estimate the background weight P_8 from data. Instead of $K^+ \rightarrow \mu^+ \nu$, we study $K_S^0 \rightarrow \pi^+ \pi^-$. For this estimate, we assume that the production and decay kinematics of K^+ and K_S^0 are approximately the same. The branching fractions are similar. To account for the smaller decay length of K_S^0 compared to $K^\pm$, we scale the volume in which the $K^\pm$ can decay (719 mm in radius and 1360 mm in half-length) by the fraction of lifetimes. 719 mm is the sum of the inner radius of the calorimeter, plus the transverse interaction length of K^+ in the calorimeter. We analyze single muon (instead of dimuon) data to account for correlations. We compare two histograms: one is p_T of pions from K_S^0's decaying in the scaled-down volume, and the other histogram is p_T of the second (in order of decreasing p_T) muon passing cuts. By this indirect method we obtain $P_8 \approx 0.041 \pm 0.010(\text{stat}) \pm 0.041(\text{syst})$.

Within errors, the two measurements of P_8 agree and we use the result from the first method.

The systematic uncertainty of P_8, ± 0.019, was taken as half the difference of 0.078 and 0.041. This value is reasonable in view of the variation of the measured P_8 with different cuts and data subsets.

From Monte Carlo simulations we obtain $P_8 = 0.047 \pm 0.034(\text{stat})$, consistent with the above.

VII. SYSTEMATIC UNCERTAINTIES OF A

We add in quadrature the following systematic uncertainties. A summary is presented in Table VI.

TABLE VI. Systematic uncertainties of the dimuon charge asymmetry A for standard cuts.

Source of error	ΔA
detector	0.00015
$e = \epsilon^+/\epsilon^-$	0.00018
prompt $\mu + K^\pm$ decay	0.00083
dimuon cosmic rays	0.00010
prompt $\mu +$ cosmic μ	0.00001
wrong charge sign	0.00018
punch-through	0.00001
Total	0.00089

Detector effects. Before averaging over magnetic field polarities, the detector introduces a dimuon charge asymmetry of ≈ 0.006 in absolute value, as discussed in Sec. IV. After averaging over magnetic field polarities (with appropriate weights), the uncertainty of the dimuon charge asymmetry due to detector geometry effects is $|A_{\text{fb}} \cdot A_{\text{det}}|$ (see Eq. (4)). As a measure of this uncertainty, we have used the largest deviation from zero, $|A_{\text{fb}} \cdot A_{\text{det}}| = 0.0049 \cdot 0.030 = 0.00015$, obtained after any of the 54 sets of dimuon cuts, for any of the three detector regions (central, forward, or all).

Inaccuracy of $e \equiv \epsilon^+/\epsilon^-$. We have obtained the ratio e by counting dimuon events with toroid polarity $\beta = 1$ and dividing by the corresponding number for $\beta = -1$. This procedure introduces no bias since we count all dimuons regardless of the charges of each muon. We take $\Delta e = 0.03$ from the largest difference between any cuts. Multiplying by the detector dimuon charge asymmetry before averaging over magnet polarities, ≈ 0.006 in absolute value, we obtain $\Delta A \approx 0.00018$.

Prompt $\mu + K^\pm$ decay. The single muon charge asymmetry of kaon decay is $a = 0.026 \pm 0.005$ as explained in Section VI. We take $P_8 = 0.078 \pm 0.023$ from Table V. The corresponding correction to A, explained in Sec. V, is $\delta A = -0.5 a P_8/A_{\text{den}} = -0.5 \times (0.026 \pm 0.005) \times (0.078 \pm 0.023)/A_{\text{den}} = -0.0023 \pm 0.0008$ ($A_{\text{den}} \approx 0.436$ is the denominator of Eq. (8)). This uncertainty on δA is by far the dominating systematic uncertainty of the entire measurement.

Dimuon cosmic rays. These are cosmic rays detected twice, once as they enter and once as they exit the D0 detector. We take $P_7 < 0.007$ from Table V. From cuts that select cosmic rays, we obtain the apparent dimuon charge asymmetry $A = -0.0095 \pm 0.0117$. Then the corresponding uncertainty of A is $< 0.007 \times 0.28 \times 0.021/A_{\text{den}} = 0.0001$ (see Table IV; $0.021 = |-0.0095| + 0.0117$).

Prompt $\mu +$ single cosmic ray. We take $P_9 < 0.0002$, see Table V. From cuts that select cosmic rays, we obtain an apparent single muon charge asymmetry $a = 0.026 \pm 0.002$. Then the uncertainty in A is $< 0.0002 \times 0.5 \times 0.028/A_{\text{den}} = 6 \times 10^{-6}$ (see Table IV; $0.028 = 0.026 + 0.002$).

Wrong local muon sign. $P_{13} < 0.001$, see Table V. Even if the asymmetry of wrong tracks is 0.1 (overestimate), the corresponding uncertainty of A is small: $<0.001 \times 0.78 \times 0.1/A_{\mathrm{den}} = 0.00018$ (see Table IV).

Punch-through. We take $P_{10} < 0.002$, see Table V. The measured charge asymmetry of tracks with $p_T > 3.0$ GeV/c is 0.0049 ± 0.0005 due to showers on matter instead of antimatter. Then the error in A is $<0.002 \times 0.5 \times 0.0054/A_{\mathrm{den}} = 1 \times 10^{-5}$ (see Table IV; $0.0054 = 0.0049 + 0.0005$).

VIII. OTHER CROSS-CHECKS

The sign of central muons was cross-checked using cosmic rays (which are charge asymmetric [1]). The sign of forward muons relative to the sign of central muons was cross-checked with J/ψ's.

The direct and reverse magnetic fields in the iron toroid were measured to be equal to within 0.1%.

We find the dimuon charge asymmetry A stable (within statistical errors) for all recorded events or events passing a set of dimuon triggers, and across the different cuts (54 sets were studied), data subsets, opposite or equal toroid and solenoid polarities, central or forward muons, or flavor creation or flavor excitation events.

IX. RESULTS

We obtain $A = 0.0005 \pm 0.0018$(stat) for opposite solenoid and toroid polarities, and $A = -0.0016 \pm 0.0019$(stat) for equal solenoid and toroid polarities (see last line in Table III). Combining these measurements we obtain

$$A = -0.0005 \pm 0.0013(\text{stat}). \quad (10)$$

We add a correction $\delta A = -0.0023 \pm 0.0008$ to A due to asymmetric $K^{\pm}$ decay (this effect is explained in Secs. VI and VII). The uncertainty of this correction dominates the systematic uncertainties of the *CP*-violation parameter. The final corrected value of the dimuon charge asymmetry is

$$A = -0.0028 \pm 0.0013(\text{stat}) \pm 0.0009(\text{syst}). \quad (11)$$

The breakdown of systematic uncertainties of A is presented in Table VI.

From the dimuon charge asymmetry A we obtain

$$\frac{\Re(\epsilon_{B^0})}{1 + |\epsilon_{B^0}|^2} = \frac{A_{B^0}}{4} \equiv f \cdot A$$

$$= -0.0023 \pm 0.0011(\text{stat}) \pm 0.0008(\text{syst}), \quad (12)$$

where

$$f = 0.814 \pm 0.105(\text{syst}). \quad (13)$$

The breakdown of systematic uncertainties of f, calculated

from information provided in preceding sections, is listed in Table VII. In comparison, recent results for $\Re(\epsilon_{B^0})/(1 + |\epsilon_{B^0}|^2)$ are -0.0013 ± 0.0029 (Particle Data Group 2006 world average [11]), -0.0003 ± 0.0020(stat) ± 0.0018(syst) from Belle [12], and 0.0004 ± 0.0014(stat) ± 0.0010(syst) from *BABAR* [13].

All preceding equations correspond to the case $\chi_s = \bar{\chi}_s$. From (8) we obtain, for the general case $\chi_d \neq \bar{\chi}_d$ and $\chi_s \neq \bar{\chi}_s$,

$$A = \frac{1}{4f}\left[A_{B^0} + \frac{f_s\chi_{s0}}{f_d\chi_{d0}}A_{B_s^0}\right]. \quad (14)$$

We measure the ratio R of like-sign to opposite-sign dimuons. For this measurement we require the invariant mass of the two muons to be either in the window 5.0 to 8.7 GeV/c^2 or 11.5 to 30 GeV/c^2. These mass cuts are designed to reduce backgrounds from same-side direct-sequential decay and backgrounds from ψ and Υ meson decays to allow a measurement of $B \leftrightarrow \bar{B}$ mixing. For this reason we set $P_4 = P_6 = 0$ for the mixing analysis. We also require dimuon triggers from a list that excludes triggers requiring opposite-sign muons. We obtain $R = 0.461 \pm 0.001$(stat) ± 0.010(syst), and $\xi = 0.229 \pm 0.001$(stat) ± 0.036(syst). The breakdown of systematic uncertainties, calculated from information provided in preceding sections, is shown in Table VIII. The final result for the mixing probability, averaged over the mix of hadrons with a b quark, is

$$\chi_0 = 0.132 \pm 0.001(\text{stat}) \pm 0.024(\text{syst}). \quad (15)$$

The agreement with the world average, 0.126 ± 0.008 [11], is a sensitive test of P_2 and f, since the largest systematic uncertainty of ξ and f are due to the same weight P_2.

Finally, we measure the tendency of μ^+ (μ^-) to go in the proton (antiproton) direction. We obtain the forward-backward asymmetry for events passing standard single and dimuon cuts:

$$A_{\mathrm{fb}} = 0.0004 \pm 0.0005(\text{stat}) \pm 0.0002(\text{syst}). \quad (16)$$

TABLE VII. Systematic uncertainties of f.

Source of error	Δf
P_2	0.084
P_7	0.002
P'_8	0.056
χ_{d0}	0.012
f_d	0.014
χ_{s0}	0.0002
f_s	0.019
ρ'	0.008
P_{13}	0.0007
Total	0.105

TABLE VIII. Systematic uncertainties of $\xi = 2\chi_0(1 - \chi_0)$. $P'_4 \equiv P_4 + P_5 + P_6$.

Source of error	$\Delta\xi$
R	0.0074
P_2	0.028
P'_4	0.015
P_7	0.0001
P'_8	0.015
P_{13}	0.0002
Total	0.036

A_{fb} is defined in Sec. IV. The systematic uncertainty is $|A||A_{\mathrm{det}}| < 0.0044 \times 0.030$. As indicated earlier, the fraction of muons from W decay in this sample is negligible.

In conclusion, the results (11) through (16), are consistent with the standard model [1], and constrain some of its extensions [3,4]. The general result (14) complements measurements at B factories [11–13], which are sensitive only to A_{B^0}, not $A_{B_s^0}$.

[1] S. Eidelman *et al.*, Phys. Lett. B **592**, 1 (2004).

[2] A. J. Buras, W. Slominski, and H. Steger, Nucl. Phys. **B245**, 369 (1984).

[3] L. Randall and S. Su, Nucl. Phys. **B540**, 37 (1999).

[4] J. L. Hewett, hep-ph/9803370.

[5] V. Abazov *et al.*, hep-physics/0503151.

[6] V. Abazov *et al.* (D0 Collaboration), Nucl. Instrum. Methods Phys. Res., Sect. A **565**, 463 (2006).

[7] S. Abachi *et al.* (D0 Collaboration), Nucl. Instrum. Methods Phys. Res., Sect. A **338**, 185 (1994).

[8] B. Abbott *et al.* (D0 Collaboration), Phys. Rev. Lett. **84**, 5478 (2000).

[9] T. Sjöstrand, L. Lönnblad, and S. Mrenna, Report No. LU-TP 01-21, 2001.

[10] R. Brun *et al.*, CERN Program Library Long Writeup W5013, 1994.

[11] W.-M. Yao *et al.*, J. Phys. G **33**, 1 (2006).

[12] E. Nakano *et al.*, Phys. Rev. D **73**, 112002 (2006).

[13] B. Aubert *et al.*, Phys. Rev. Lett. **96**, 251802 (2006).